OBSERVATIONS AND MODELLING OF THE ON-ICE AND OFF-ICE AIR FLOW OVER THE NORTHERN BALTIC SEA

TIMO VIHMA[1]* and BURGHARD BRÜMMER[2]
[1]*Finnish Institute of Marine Research, P.O. Box 33, FIN-00931, Helsinki, Finland;*
[2]*Meteorologisches Institut, Universität Hamburg, Germany*

(Received in final form 26 July 2001)

Abstract. Two cases of on-ice and off-ice air flow characterizing the opposite weather situations over the ice-edge zone in the northern Baltic Sea are analysed on the basis of aircraft observations, and modelled using a two-dimensional mesoscale model. The stable boundary layer (SBL) during the on-ice flow exhibited little thermal modification, but a low-level jet (LLJ) was generated at the 250-m high top of the SBL. In the model, the LLJ was associated with inertial oscillations in space, while the baroclinicity explained the shape of the wind profile well above the SBL. Although the observed LLJ was most pronounced over the ice, the modelling suggests that it was not generated by the ice edge but by the coastline some 400 km upwind of the ice edge, where a much more drastic change in the thermal stratification and surface roughness took place. The generation, maintenance, and strength of the LLJ were very sensitive to the parameterization of turbulent mixing in the SBL. In the case of the off-ice flow, the modification of the air mass and the development of a convective boundary layer (CBL) both over the ice and open sea were reasonably well modelled. Sensitivity runs suggested that it was essential to take into account the effects of subgrid-scale leads, a forest in the archipelago (which was crossed by the air flow), and water vapour condensation into ice crystals. The heat flux from leads was particularly important for the heat budget of the CBL, and the observed growth of the CBL was partly due to the effective mixing over the rough and relatively warm forest.

Keywords: Aircraft observations, Baltic Sea, Low-level jet, Mesoscale modelling, Off-ice flow, On-ice flow.

1. Introduction

The Baltic Sea influences the overlying atmospheric boundary layer (ABL) via the turbulent and radiative surface fluxes, and the degree of influence depends on the state of the surface (open water or sea ice) and on the origin of the flow (off-land, off-ice, off-sea). In winter, the maximum extent of sea-ice cover is from 10 to almost 100% of the Baltic Sea area, with large inter-annual variations. An unstable stratification prevails in the atmospheric surface layer in winter as long as the surface is ice-free. When ice has been formed, a stable stratification is typical over a compact ice cover. The ice cover is, however, often fractured, and the upward sensible and latent heat fluxes from leads modify the properties of the ABL. Offshore winds bring continental air masses over the sea, which may be

* E-mail: vihma@fimr.fi

Boundary-Layer Meteorology **103:** 1–27, 2002.

open or covered by a compact or fractured ice field, and the modification occurring depends on the state of the surface. Analogously to offshore winds, off-ice winds bring cold air from the sea ice over the open ocean, where a convective boundary layer develops. In the reverse situation, on-ice winds bring warm and moist air over the ice, where downward turbulent fluxes consequently occur.

The modification of the ABL over the Baltic Sea is important for the weather and climate. Especially in winter with the sea open, the region may be very baroclinic, leading to the formation or intensification of mesoscale cyclones. In addition, evaporation from the open sea is usually large. The lack of routine observations over the sea makes weather forecasting difficult during conditions of significant ABL modification. During cold air outbreaks over the open water, convective snowbands may occur, and the location of the sea-ice boundary has a strong effect on their development (Andersson and Gustafsson, 1994). An extreme case occurred on 4–7 December 1998, when up to 1.4 m of snow accumulated in Gävle, on the eastern coast of Sweden (Andersson and Michelson, 1999).

The properties of the ABL over the Baltic Sea ice cover have not been extensively studied. Joffre (1982, 1983) addressed the form drag over sea ice and the influence of stability and baroclinity on the wind profiles, Uotila et al. (1997) presented statistics of the ABL structure based on rawinsonde soundings over sea ice in the Gulf of Bothnia, and Launiainen et al. (2001) analyzed the flux-profile relationships over land-fast sea ice. The interaction of sea ice and the atmosphere in a regional scale model has been addressed by Gustafsson et al. (1998). Considering the Arctic and Antarctic sea ice, several authors have addressed both off-ice (Raasch, 1990; Lüpkes and Schlünzen, 1996; Brümmer, 1997; Hartmann et al., 1997; Renfrew and Moore, 1999; Olsson and Harrington, 2000) and on-ice (Andreas et al., 1984; Bennett and Hunkins, 1986; Brümmer et al., 1994) flows.

In this paper, one case of on-ice and another of off-ice air flow characterizing the opposite weather conditions over the northern Baltic Sea are analyzed on the basis of aircraft observations. The data were obtained during a field experiment of the Baltic Air-Sea-Ice Study (BASIS; Launiainen, 1999). We present observations on the ABL modification, and a two-dimensional mesoscale model is then applied to simulate the observed modification and to study the sensitivity of the modification on fetch characteristics and turbulence parameterizations.

2. BASIS Field Experiment

2.1. MEASUREMENTS

The experimental part of this study was based on data gathered by the German Falcon research aircraft over the ice-covered and open part of the Gulf of Bothnia. During the period from 27 February to 6 March, 1998, six flight missions were flown (Brümmer and Müller, 1999). Two of them, that on 27 February in a warm

on-ice air flow situation, and that on 5 March in a cold off-ice air flow situation, are presented in this paper. The operations base was situated at the airfield at Kokkola in Finland.

On both missions the flight pattern was arranged along the mean wind direction (Figure 1). It consisted of a sequence of vertical profiles (referred to by P1–P7) in the lowest 1–3 km and of horizontal flight legs at different levels in the boundary layer. The horizontal legs were arranged as vertical stacks (referred to by I–III) oriented perpendicular to the wind direction. Figure 1 shows for the two flight missions three vertical stacks with 4 and 3 horizontal legs, respectively. Typically, the vertical profiles were flown on both sides of the vertical stacks. The transits from one stack to another were flown at low levels between 20 and 90 m, as were also the lowest legs within the stacks. The flight missions of 27 February and 5 March lasted for 3 and 1.8 hours, respectively. In addition, rawinsonde soundings were made during the BASIS field experiment four times a day at six coastal locations around the Gulf of Bothnia, and surface-layer observations were made at several sites on the sea ice (Launiainen, 1999). We use them as supporting data.

2.2. Data obtained

The Falcon was equipped with a gust probe system to measure the turbulent fluctuations of the three wind components (u, v, and w), air temperature (T), and water vapour mixing ratio (m) with a time resolution of 0.01 s. With a typical flight speed of 100 m s^{-1} this corresponds to a spatial resolution of 1 m. In addition, the Falcon was equipped with radiation sensors to measure the surface temperature and the shortwave and longwave radiation fluxes from above and below with a time resolution of 0.1 s. Furthermore, several cloud-sensing instruments were installed, but the results from these will not be used in this paper. For details of the Falcon instrumentation, see Brümmer and Müller (1999).

The vertical structure of the boundary layer was obtained from the wind, temperature and humidity profiles and the vertical fluxes of heat, moisture and momentum, while the radiation fluxes were taken from the horizontal legs. The properties of the boundary layer in a vertical cross-section over the ice, the ice-edge zone, and the open water were documented in this way.

The Bay of Bothnia (the northernmost part of the Gulf of Bothnia) was mostly covered by sea ice during the experiment, but the cover was fractured, with typical ice concentrations of 80–100%. In addition, a 10–50 km wide coastal margin on the Finnish side of the Bothnian Sea was covered by ice. The data on the ice conditions were based essentially on the digitized ice charts of the Finnish Institute of Marine Research (FIMR) and the Swedish Meteorological and Hydrological Institute (SMHI), which also analyzed the ice concentrations from Radarsat images. An overview of the conditions is presented in Figure 1. More detailed local-scale information was obtained from the surface temperature and albedo measured by the Falcon.

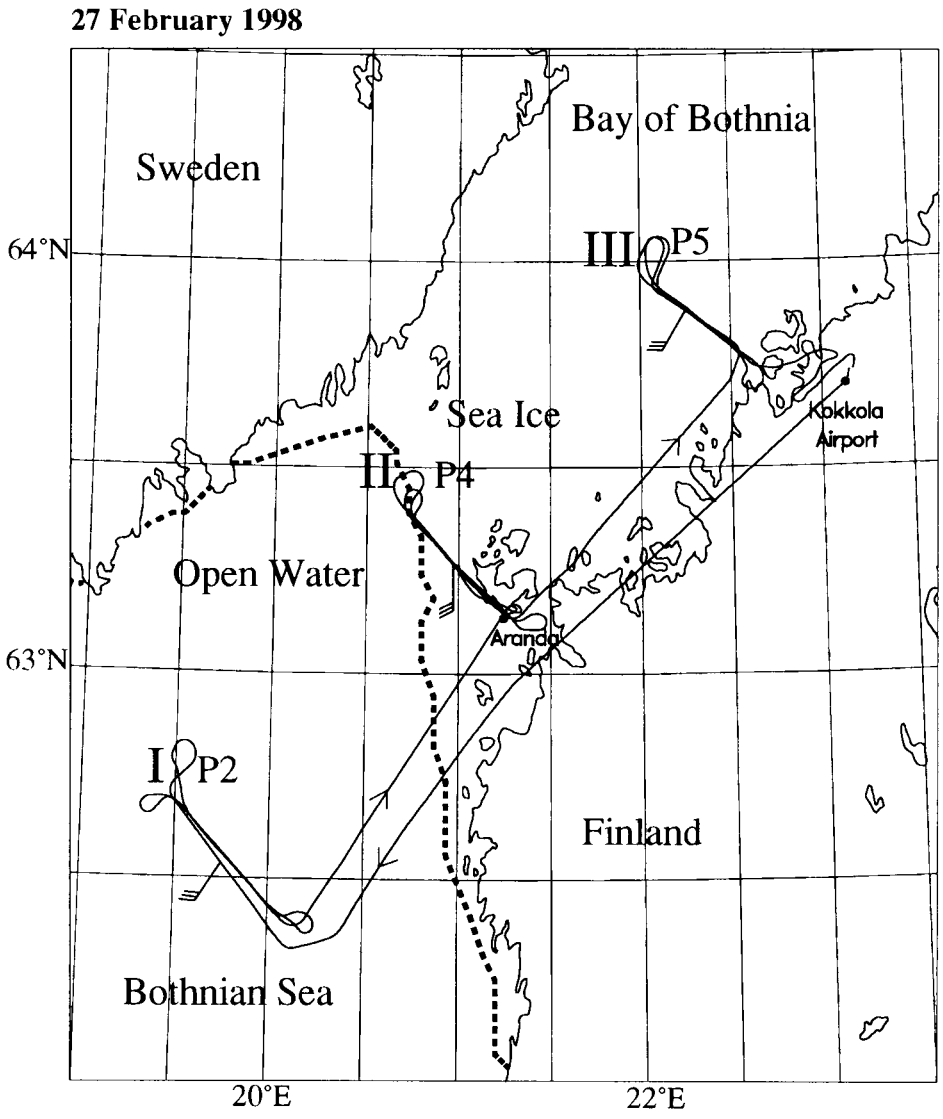

Figure 1a.

Figure 1. Flight patterns of the Falcon research aircraft on (a) 27 February and (b) 5 March 1998. Locations of vertical stacks (I–III) and profiles (P1–P7) used in this paper are marked. The approximate position of the ice edge is dashed, and the near-surface wind is marked at each stack. The operations base was at Kokkola airport.

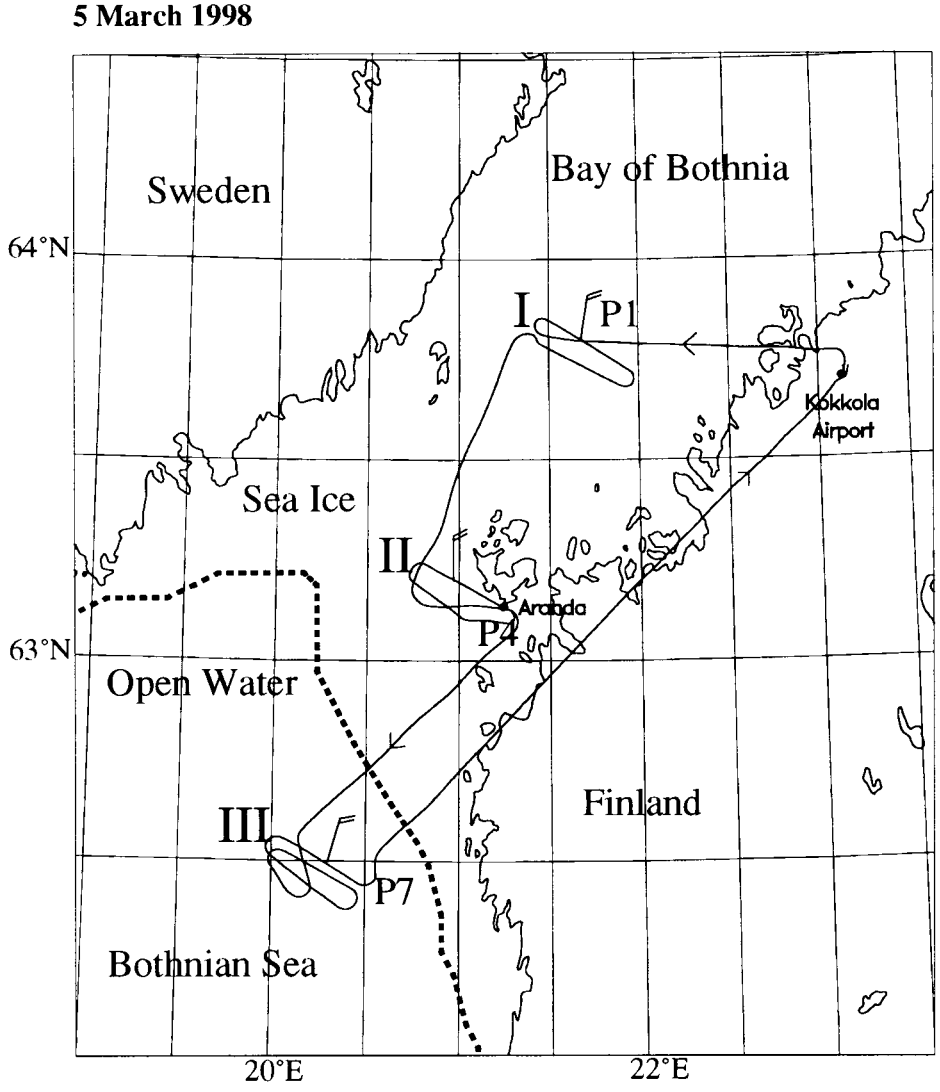

Figure 1b.

3. Analyses Based on Aircraft Measurements

The ABL modification as measured in two cases (on-ice and off-ice air flow) by the Falcon research aircraft is presented below. Figure 2 shows the 1200 UTC surface pressure fields on 27 February and 5 March 1998. On 27 February, an extensive low with its centre close to the Lofote Islands produced a southerly to south-westerly airstream over the region of the Gulf of Bothnia. Air temperatures were around +2 °C. On 5 March, the experimental area was influenced by a depression with its centre over the White Sea. The depression had moved over the Gulf of Bothnia

a)

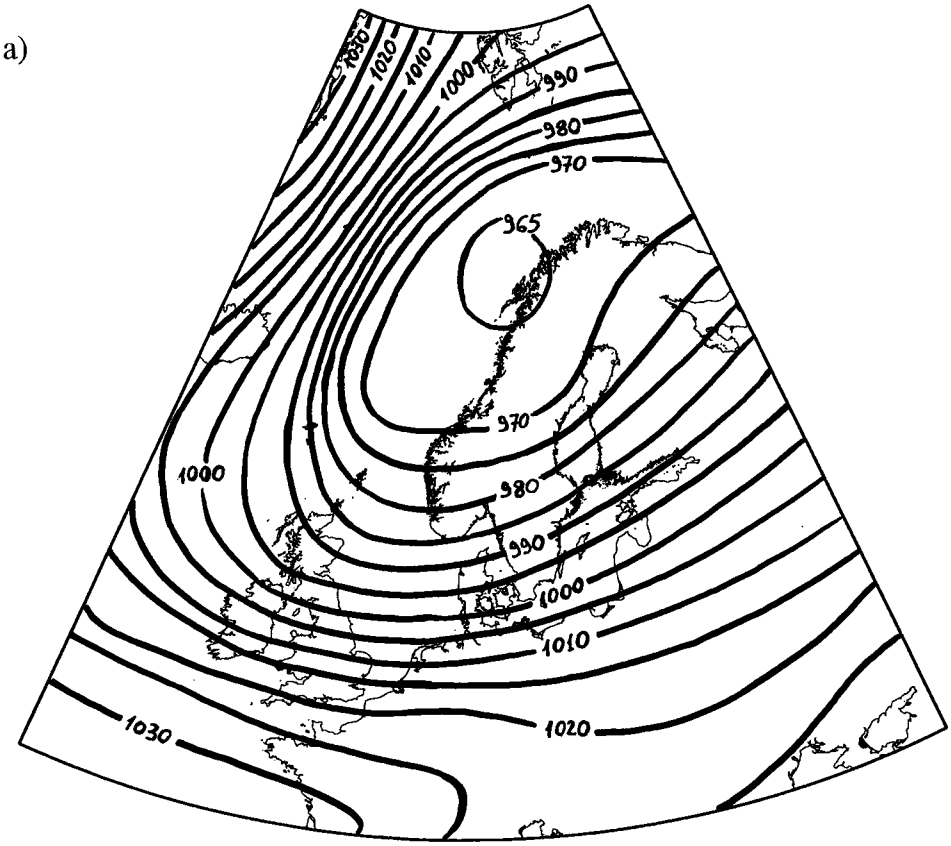

Figure 2a.

Figure 2. Surface pressure fields (hPa) at 1200 UTC for (a) 27 February and (b) 5 March 1998 redrawn from the analyses of the German Meteorological Office.

from the west to south-west on the previous day and gave rise on its rear flank to cold air advection from the north to north-east. The air temperatures were between -10 and -15 °C.

3.1. ABL MODIFICATION ON 27 FEBRUARY, 1998 DURING ON-ICE AIR FLOW

This day was characterised by weak temperature differences between the ice and the water surface. The mean surface temperature measured at stack I (see Figure 1) over open water was T_w = 1.1 °C, and the ice surface temperature T_i was -0.3 °C at stack II and -0.2 °C at stack III. The high T_i values were a consequence of the warm air advection with low-level air temperatures around $T = +2$ °C. The air-surface temperature difference ($T - T_{sfc}$) was thus positive all over the area. Due to the strong wind of about 14 m s^{-1} (at the height of 10 m), the surface-layer

b)

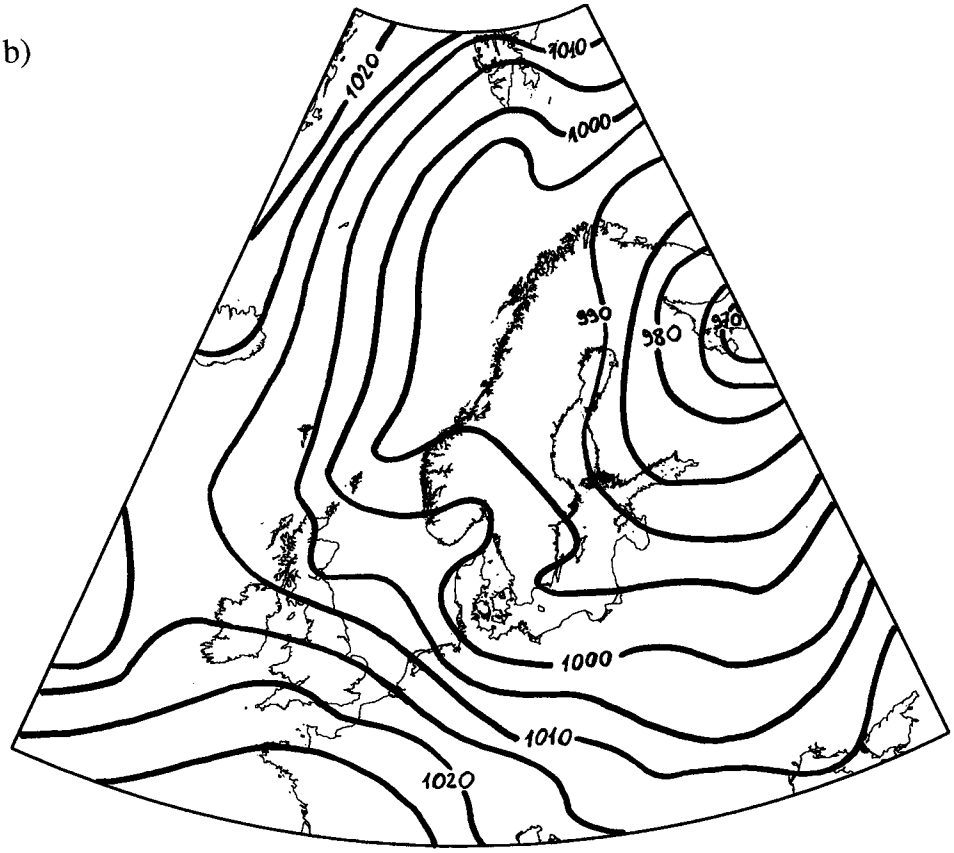

Figure 2b.

stratification was slightly stable: z/L $\approx$ 0.03 (where L is the Obukhov length and z = 10 m).

Figure 3 shows the profiles of T, the water vapour mixing ratio m, the wind speed V, and the wind direction DD measured during the vertical profile flights P2, P4, and P5, which were located approximately along an air flow trajectory (see Figure 1). The distances P2–P4 and P4–P5 were both about 95 km. The air mass modification over a total distance of about 190 km was rather small due to the weak contrast between T_w and T_i. Over water as well as over ice, an isothermal layer or a weak inversion was present in the lowest 200 to 400 m. Above this stable layer the air was well-mixed, and winds were very high on this day all over the area. The stable layer was characterised by large wind shear and a pronounced low-level jet (around 20 m s^{-1}) at its top.

Due to the combined effect of the warm air advection and temperatures above freezing, the sea and ice surface temperatures were nearly the same, and thus the air mass modification caused by the transition from water to ice was small. Interesting

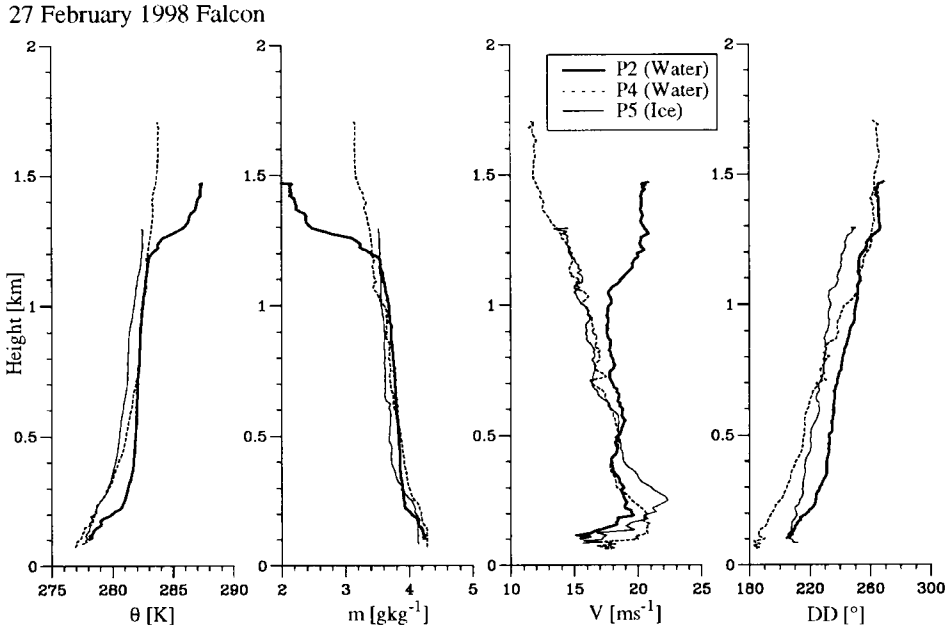

Figure 3. Vertical profiles of the potential temperature θ, water vapour mixing ratio m, wind speed V and wind direction DD measured by the Falcon research aircraft on 27 February, 1998, at P2, P4 and P5 (see Figure 1).

wind features were found, however, in the stably-stratified shallow boundary layer, and the processes causing them will be studied by model simulations in Section 5.

3.2. ABL MODIFICATION ON 5 MARCH, 1998 DURING OFF-ICE AIR FLOW

This day was characterised by large temperature differences between the ice and the water surface. The mean surface temperatures measured over the ice at stacks I and II (see Figure 1), which were located ahead of the ice edge ($x = 0$) at $x = -138$ km and $x = -62$ km, were $T_i = -11.2$ °C and -10.9 °C, respectively. The water surface temperature at stack III at $x = 15$ km was about $T_w = 0.7$ °C. The low T_i values were a consequence of cold air advection which started with $T = -12.9$ °C at stack I and of the negative net radiation $R_N = -30$ to -60 W m^{-2} under clear sky conditions over the ice during the night. During the time of the flight mission, between 1100 and 1200 local time, R_N was slightly positive, from 10 to 20 W m^{-2}, at stacks I and II.

Figure 4 shows the T, m, V, and DD profiles measured at positions P1, P4, and P7 (see Figure 1), which were again roughly located along an air-flow trajectory. The distances P1–P4 and P4–P7 were both approximately 80 km. Over the ice the cloud cover varied from 3 to 8 octas, and the depth of the boundary layer increased downwind, from 300 m at P1 to 470 m at P4, and further to about 550 m

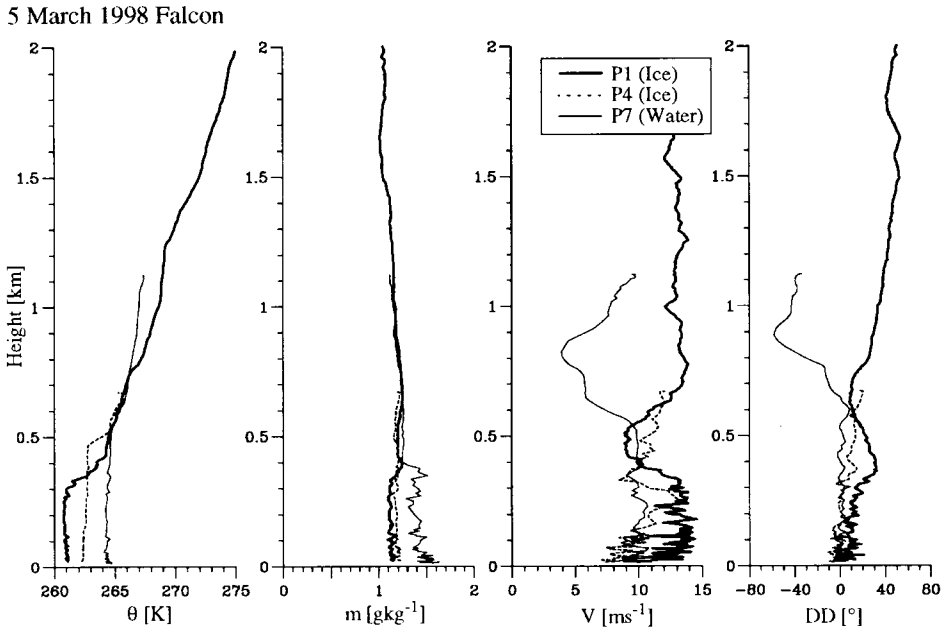

Figure 4. As Figure 3, but for 5 March, 1998, at P1, P4 and P7.

at P7, where the cloud layer was between 400 m and 1200 m. Along with the increase in the depth of the boundary layer, its temperature also increased. The air was well-mixed and the low-level temperature was always lower than the surface temperature. The low-level air temperature (at a height of 30 m) was −13.0 °C at P1, −11.9 °C at P4, and −8.9 °C at P7. Thus, the mean air-surface temperature difference $T - T_{sfc}$ was −2 to −1 K over the ice at stacks I and II, and −9.5 K over the water at stack III. The wind was from the north-north-east in the entire area, and decreased slightly from north to south (13 m s^{-1} at P1/stack I, 10.5 m s^{-1} at P4/stack II, 9 m s^{-1} at P7/stack III). V and DD were well-mixed throughout the entire boundary layer over the ice, but only in the subcloud layer over the water. Here, in accordance with the stronger cold-air advection, the wind backed and decreased with height.

Due to the combined effects of the cold air advection and the nighttime negative net radiation on 5 March, 1998, the ice surface temperature was about 10 K cooler than the sea surface temperature. Even over the ice, the air temperature was slightly below that of the ice surface. This was partly due to the conductive heat flux through the ice (about 15 W m^{-2}; Cheng et al., 2001). Hence, the boundary layer was unstably stratified both over the ice (weakly) and over the water (strongly). The surface heat flux was some 4 to 9 times larger over the water than over the ice (see Figure 9).

The two cases of ABL modification during on-ice and off-ice air flow presented here are typical of the two reverse situations occurring in wintertime over the Gulf of Bothnia in the region of the ice edge zone.

4. Mesoscale Model

In order to complement our understanding of the physics of on-ice and off-ice flows and to verify the parametrization schemes for stable and unstable conditions over sea ice and its edge zone, the ABL flow over the Gulf of Bothnia was simulated using a two-dimensional numerical model. In the hydrostatic boundary-layer model of the Department of Meteorology, University of Helsinki, the flow is forced by a large-scale pressure gradient represented by the geostrophic wind. The model has 92 points in the horizontal and 50 in the vertical. The vertical coordinate is terrain-following, modified σ; $\sigma = (p - p_t)/(p_s - p_t)$, where p is pressure, and subscripts s and t refer to the surface and model top, respectively. The vertical grid has a quasi-logarithmic spacing with the lowest levels at approximately 1.5, 4, 8, 15, and 24 m; the upper boundary conditions are applied at 3 km, where the wind becomes geostrophic. The grid length is 2 km and the time step accordingly 4 s. (For the case of 27 February, 4 km and 8 s were used, because a larger model domain was required.) All fluxes vanish at the model top, and no-gradient conditions are applied at the lateral boundaries. Vertical diffusion is solved by an implicit method, and instead of explicit horizontal diffusion, a weak lowpass filter is applied to all fields. The equations of the model dry dynamics are as given in Alestalo and Savijärvi (1985), but the physical parameterizations are as in Savijärvi (1997) with the humidity, clouds, and a radiation scheme included, and the thermodynamic 15-layer sea ice model of Launiainen and Cheng (1998) is coupled to the atmospheric model.

For the present simulations, we improved the description of turbulence by applying a non-local closure with a parameterization for the countergradient transport of heat and moisture in convective conditions. Accordingly, the turbulent kinematic heat flux ($\overline{w'\theta'}$) is parameterized as

$$\overline{w'\theta'} = -K\left(\frac{\partial\theta}{\partial z} - \gamma_\theta\right),$$

where θ is the air potential temperature, z is the height, and γ_θ is the countergradient transport term, which we calculate according to Holtslag and Moeng (1991). An analogous formula is applied for the air moisture. The vertical diffusion coefficient $K = l^2(\mathrm{d}U/\mathrm{d}z)f(\mathrm{Ri})$, where U is the wind speed. The mixing length $l = kz/(1 + kz/\epsilon)$; its asymptotic limit ϵ is discussed in Sections 5 and 6; here $f(\mathrm{Ri})$ is an empirical function depending on the Richardson number Ri. In unstable stratification conditions, $f(\mathrm{Ri}) = (1 - 16\mathrm{Ri})^{1/2}$ for momentum and $f(\mathrm{Ri}) = (1 - 64\mathrm{Ri})^{1/2}$ for heat and moisture, and in stable stratification conditions,

max(0.1, 1 − 5Ri) is used for momentum, heat, and moisture (Savijärvi, 1991). When calculating the turbulent surface fluxes, we describe the stability effects using the universal functions of Högström (1988) in unstable cases and those of Holtslag and de Bruin (1988) in stable cases. The surface of each grid interval was divided into sub-sections of ice and open water on the basis of the observed ice concentration. The grid-averaged surface fluxes of heat and moisture were then calculated as area-averages of the local fluxes applying the (basic) mosaic method (Vihma, 1995), while a regional roughness length (Mai et al., 1996) was used to calculate the momentum flux.

This model has previously been used in several studies of mesoscale circulation systems, including cases over the Baltic Sea (Savijärvi and Alestalo, 1988; Vihma and Savijärvi, 1991) and over polar sea-ice margins (Vihma and Kottmeier, 2000). Savijärvi (1991) validated the model against an extensive boundary-layer data set in both convective and stable conditions.

5. Modelling of the On-Ice Flow on 27 February, 1998

The on-ice flow observed on 27 February, 1998 was modelled applying the two-dimensional mesoscale model. The surface boundary conditions were set as follows. On the basis of the FIMR and SMHI ice charts, the surface between P4 and P7 was estimated to be a mosaic of ice and water with an open water fraction of 0.2 (Falcon data suggested a lower open water fraction, but the Falcon's route from P4 to P7 was much closer to the coast than the direct air- mass trajectory.) We used 0.3 m as an ice thickness and 0.02 m as a snow thickness, but this case was not sensitive to these values.

On 27 February, the thermal difference between the open sea and the sea ice was small, and therefore the modification in the air temperature remained small. This was a common feature in the various simulations presented below. Although cooling was observed over the ice in the whole ABL and above it (Figure 3), the model only produced cooling in the lowest 150 m layer, which was directly affected by the downward turbulent heat flux. The observed cooling extending far above the ABL seems to be due to reasons other than the direct influence of the ice surface on the ABL. Hence, in the following we concentrate on the slightly stable ABL and the generation of the low-level jet (LLJ). With respect to the inflow boundary conditions and the simulation time, two different strategies were used. These are discussed in Sections 5.1 and 5.2.

5.1. Model domain covering the Falcon flight region

First, we included in the model domain only the region where the Falcon flights took place. The surface was either open water or sea ice with leads. The boundary-layer flow was forced by a geostrophic wind of 19 m s^{-1} based on the surface

pressure field. In the first simulations it was kept constant in height, i.e., a barotropic atmosphere was assumed. The observed profiles of the wind, temperature, and humidity at P2 (Figures 1 and 3) were given as the initial inflow conditions for the model, and the model results were compared with the observed profiles at the ice edge (P4) and 95 km downwind of it (P5). The comparison of model results with the observations at P4 was made using the model fields after a 1.5-h long simulation, corresponding to the time required for the air mass to reach P4 from P2 with a wind speed 18 m s^{-1}. The analogous time for P5 was 3 h. The time differences between the Falcon observations at P2, P4, and P5 were approximately the same.

A LLJ was observed over the ice (Figure 3), and it was found that the development of the LLJ in the model was very sensitive to the parameterization of turbulent mixing. Applying the parameter values $f(\mathrm{Ri}) = \max(0.1, 1 - 5\mathrm{Ri})$ and $\epsilon = 150$ m, no LLJ was produced in the model at either P4 nor P5. A successful simulation was only possible with far less turbulent mixing in the boundary layer. Considering ϵ, we relate it to the boundary-layer height (h_{ABL}): $\epsilon = 0.08 \times h_{\mathrm{ABL}}$, and for the dependence on the Richardson number, the relation $f(\mathrm{Ri}) = \max(0.01, 1 - 10\mathrm{Ri})$ produced the best results (Figure 5). The lower limit for $f(\mathrm{Ri})$ was more important than the factor of Ri. The stability dependence of the surface drag coefficient was not important in this case, with 10 m/L ≈ 0.03.

Sensitivity tests were also made with respect to the effect of spatial variation in the surface roughness. It has been demonstrated by Källstrand (1998) that the generation of an LLJ over the Baltic Sea in summer is sensitive to the change in surface roughness between the land and sea. In our case, however, the roughness change between the open sea (Wu, 1980) and the ice was small (z_0 from 0.3×10^{-3} to 1.0×10^{-3} m) compared to the roughness change between the open sea and a land surface. A control simulation was made with the maximum roughness change between the open sea and ice, within the range of its uncertainty, i.e., we applied a smaller wind-dependent estimate for the open sea (Smith, 1988, yielding $z_0 = 0.1 \times 10^{-3}$ m) and a higher estimate for the sea ice ($z_0 = 5 \times 10^{-3}$ m). It produced, however, results similar to those in the basic run.

There was at least a weak LLJ present in all three observed vertical profiles at P2, P4, and P5 (Figure 3c). Thus, having the wind profile at P2 as an initial inflow boundary condition for the model, we in fact simulated the development of the LLJ but not its initial generation. The above-mentioned model runs were 1.5 and 3 h long, corresponding to the time required for the air mass to reach P4 and P5, respectively. An additional 12-h long simulation was made, running the model into a steady state (applying the parameter values favouring the jet occurrence: $\epsilon = 0.08 \times h_{\mathrm{ABL}}$ and $f(\mathrm{Ri}) = \max(0.01, 1 - 10\mathrm{Ri})$). No LLJ was present in the results. This indicates that in the 1.5-h and 3-h simulations we only had modelled the advection of an air mass having a LLJ, but that the LLJ was not a stable feature in the model. This suggests that the roughness and stability differences between the open sea and sea ice were not large enough to maintain the LLJ (after the air

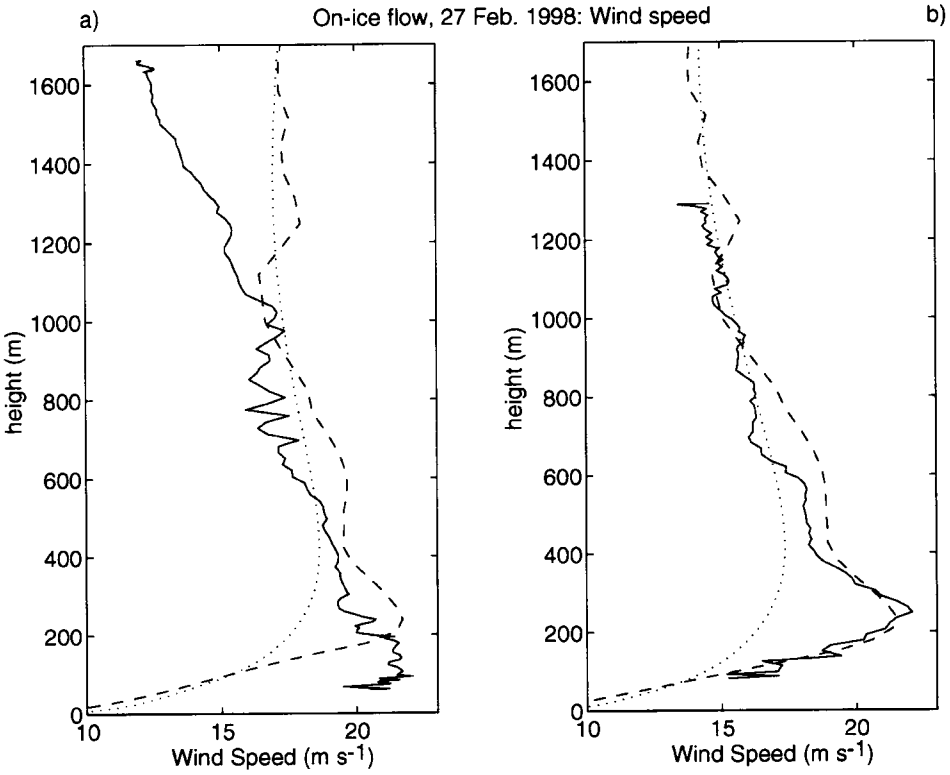

Figure 5. Observed (continuous line) and modelled wind speed profiles at (a) the ice edge and (b) 95 km downwind over the ice during the on-ice flow on 27 February, 1998. The model results with the optimal parameterizations (see text) are drawn as a dashed line, and those with the parameterizations producing more mixing as a dotted line.

mass with the initial LLJ had been advected out of the model domain). The air mass must, however, have had its origin over a land surface (see Figure 2), and the consequences of this will be studied next.

5.2. Model domain including a land surface

To understand the generation of the LLJ, we made a model run including a land surface at the upwind coast. The trajectory of the air mass observed at P2 was estimated by analyzing the 0600 and 0900 UTC wind fields of the Mesoscale Analysis system (MESAN; Häggmark et al., 2000) of the SMHI. It appeared that the air mass had departed from the Swedish coast at approximately 18.0°E, 60.5°N about 3 hours before arriving at P2. Accordingly, a patch of land surface was added to the model domain, followed by 282 km of open water upwind of P2 (i.e., upwind of the ice edge there was a total of 378 km of open water). For the upwind boundary conditions we used the MESAN values of 80% for relative humidity (constant

with height), and 4 °C for the land surface and 2-m air temperature, and applied a constant lapse rate of 7.5 K km^{-1}. The initial inflow wind profile was set as an Ekman-Taylor spiral. The patch of land surface was set to be 40 km long to allow the ABL to adjust to the surface conditions. The land surface z_0 was set to 0.5 m, and $\epsilon = 0.08 \times h_{\mathrm{ABL}}$ and $f(\mathrm{Ri}) = \max(0.01, 1 - 10\mathrm{Ri})$ were applied. The model was then run for 12 h to reach a steady state. The flow was again forced by a geostrophic wind constant in height.

The resulting wind profiles at P2, P4, and P5 included an LLJ (dashed lines in Figure 6) that fitted the observations reasonably well. The LLJ is, however, too pronounced at P2, and the jet core is too high at P4. Contrary to the observations, the jet core height slightly decreases from P4 to P5. In the model, this is in accordance with the slightly decreasing height of the stable boundary layer, which often coincides with the jet core height (Mahrt, 1981). In the observations, the increased wind speeds in the lowest 200 m at P4 may have resulted from channelling of the wind over the narrowest part of the Gulf of Bothnia, because of the land-sea roughness difference (Launiainen and Laurila, 1984).

In the model results, the LLJ is clearly a spatial feature: it is stationary, it does not exist over the upwind land surface, and it is most pronounced 500 km downwind of the coast. This follows from the theory of Thorpe and Guymer (1977) that the maximum LLJ occurs after half an inertial period, i.e., after 6.7 h at a latitude of 63°. With a wind speed of 20 m s^{-1} advecting the air mass, this corresponds to a distance of 482 km. Further, it was confirmed by a 120-h long control run that the jet did not evolve in time, and is thus not associated with inertial oscillations in time (as with the classical nocturnal jet).

In the barotropic simulations described above, the wind speed is far too high in P4 and P5 in the layer upward of 400–500 m. In order to determine the effect of baroclinicity, we estimated the horizontal temperature gradient on the basis of the BASIS rawinsonde soundings at six stations around the Gulf of Bothnia (Launiainen, 1999), and calculated the thermal wind. The result, averaged over the area of the aircraft observations, corresponds to a thermal wind of 11 m s^{-1} towards south-west between the heights of 500 and 2300 m. The previous model run was repeated with this height-dependent geostrophic forcing, and the results are shown in Figure 6 (dotted lines). We see that the shape of the wind profile well above the SBL is now fine in P4 and P5. In P2 the modelled upper winds are too low. This is because the horizontal temperature gradient was weaker at P2, but we had to apply the mean value everywhere since the mesoscale model does not allow a horizontally varying geostrophic forcing.

The observed and modelled vertical fluxes of sensible heat (H), latent heat (E), and momentum (τ), calculated from the horizontal flight legs at stacks I, II and III, are displayed in Figure 7. In accordance with the stable stratification, H is negative, with values around -20 W m^{-2} at a height of 90 m, and decreases in magnitude with height. Above 500 m, in the well-mixed layer, H is close to zero. The same profile shape holds for E and τ: the largest fluxes occur near the surface

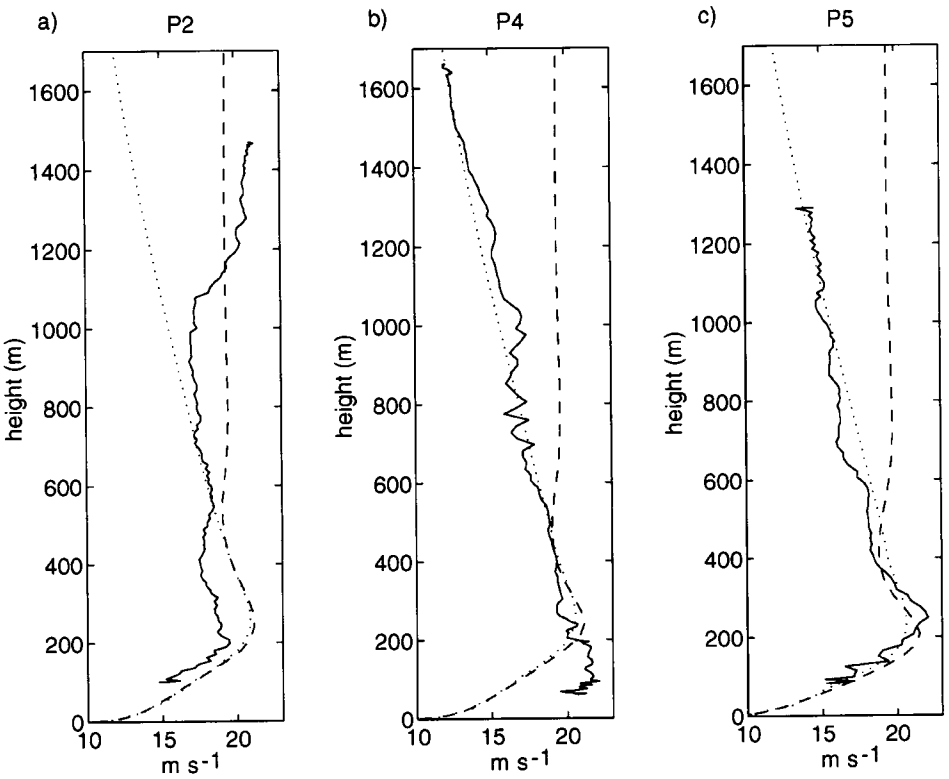

Figure 6. Observed (continuous lines) and modelled wind speed profiles at (a) 95 km upwind of the ice edge, (b) the ice edge, and (c) 95 km downwind over the ice during the on-ice flow on 27 February, 1998. The model included a 40-km-long patch of land surface with its coastline 378 km upwind of the ice edge. The barotropic model results are show as dashed lines, and the baroclinic ones as dotted lines.

and decrease to small values at the top of the stable layer. The modelled sensible heat flux is reasonably well reproduced, as is the latent heat flux at stacks I and II. The model, however, indicates a downward (negative) latent heat flux in the lowest 70 m at stack III over the ice. The modelled momentum fluxes are too small, particularly at stacks II and III. It seems that the LLJ was not too sensitive to the vertical profile of the modelled momentum flux. Of primary importance was the fact that the model reproduced the strong decrease in τ from the surface to the height of the jet.

To assess the accuracy of the aircraft-based fluxes, we compared them with the flux measurements made at three surface stations on the sea ice close to R/V Aranda, Kokkola (Figure 1), and Umeå (at the Swedish coast). For the six flight missions during BASIS, nine aircraft passages close to the three ice stations at distances less than 25 km and at altitudes below 30 m were selected for comparison. The sensible heat flux difference was: $H_{Falcon} - H_{IceStation} = -0.4 \pm 3.0$ W m^{-2}

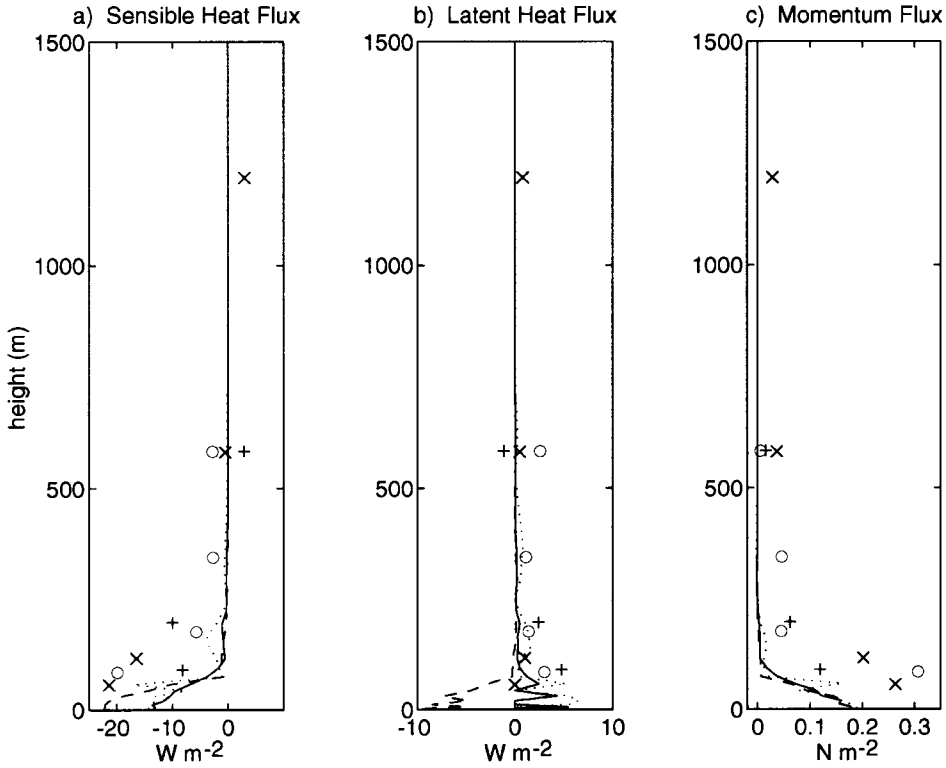

Figure 7. Observed (stack I: plus; II: cross; III: circle) and modelled (stack I: dotted lines; II: solid lines; III: dashed lines) vertical profiles of (a) sensible heat flux, (b) latent heat flux, and (c) momentum flux during the on-ice flow on 27 February, 1998. See Figure 1 for the locations of the stacks.

(mean and standard deviation) for the range -30 W m^{-2} $<$ H $<$ 30 W m^{-2}. The latent heat flux could not be compared, because it was not measured at the ice stations. The momentum fluxes compared as: $\tau_{\text{Falcon}} - \tau_{\text{IceStation}} = 0.01 \pm 0.05$ N m^{-2} for the range $0.00 < \tau_{\text{Falcon}} < 0.34$ N m^{-2}. It can therefore be concluded that the aircraft fluxes are of acceptable accuracy to be taken as a reference for the validity of the model simulations.

6. Modelling of the Off-Ice Flow on 5 March, 1998

The off-ice flow on 5 March, 1998, was modelled applying inflow vertical profiles of wind speed, air temperature, and humidity over ice as observed by the aircraft at site P1 (Figures 1 and 4). The flow was forced by the observed geostrophic wind of 8 m s^{-1} at a height of 3 km. This value was taken from the rawinsonde soundings made at R/V Aranda (close to P4) and Kokkola (close to P1) between 0600 and

1200 UTC. The model was run for 12 h (with the solar elevation angle fixed to its noon value) to reach a steady state.

6.1. REFERENCE RUN

The surface boundary conditions were set as follows. The surface was estimated to be a mosaic of ice and water for the first 138 km from the inflow boundary, with an open water fraction of 0.2 between P1 and P4, zero over the land-fast ice 16 km downwind from P4, and then 0.3 until the southernmost ice edge. In fact, the Falcon data on surface temperature and albedo suggested a higher open water fraction of 0.4 between P1 and P4, but the air-mass trajectory from P1 to P4 was closer to the Finnish coast than the Falcon flight leg had been (Figure 1), and both the FIMR and SMHI ice charts suggest lower open water fractions there. According to the surface-based observations (Vihma et al., 1999), the ice thickness was set to 0.3 m and the snow thickness to 0.02 m. The small snow thickness was also supported by visual observations from the Falcon, which indicated the occasional presence of bare ice (Brümmer and Müller, 1999). Following Mai et al. (1996), the effective roughness length was set to 0.005 m for the deformed sea ice between P1 and P4. Between P4 and P7 the surface was mostly smooth land-fast ice, and a roughness length of 1.4×10^{-4} m measured at the R/V Aranda ice station (Launiainen et al., 2001) was applied.

Below the air-mass trajectory from P1 to P4 there were a few islands, with a total length of 16 km (Figure 1). The islands were covered by pine and spruce forest, and hence their energy budget was very different from that of the sea ice. We therefore developed a simple subroutine to calculate the energy budget of the forest. Since the forest was dense, with a tree cover of over 70%, the presence of snow on the surface had little effect on the albedo, and we set the forest albedo to 0.15 (Ni and Woodcock, 2000). Following the empirical results of Gryning et al. (2001) on the wintertime energy budget of a boreal forest, we neglected the latent heat flux from the trees and assumed that the upward sensible heat flux at the level of the forest top (approximately 20 m) equals the net radiation during day time. The air inside the forest was completely mixed in the model.

According to the aircraft observations, in addition to the liquid water cloud droplets, ice crystals were present over almost the entire experimental area (Brümmer and Müller, 1999). In modelling the condensation and cloud formation, the saturation specific humidity was therefore calculated as an average of the saturation humidities with respect to water and ice, using the equations of Buck (1981). This was, of course, just a rough parameterization in lieu of a microphysical cloud model. In the model results the cloud cover was unbroken, and the cloud base height increased from 300 to 450 m between P1 and P7. The latter was approximately in agreement with the observations (270 to 390 m), but the modelled cloud layer did not become as thick as the observed one. The boundary layer heating in the model was, however, not sensitive to the cloud thickness.

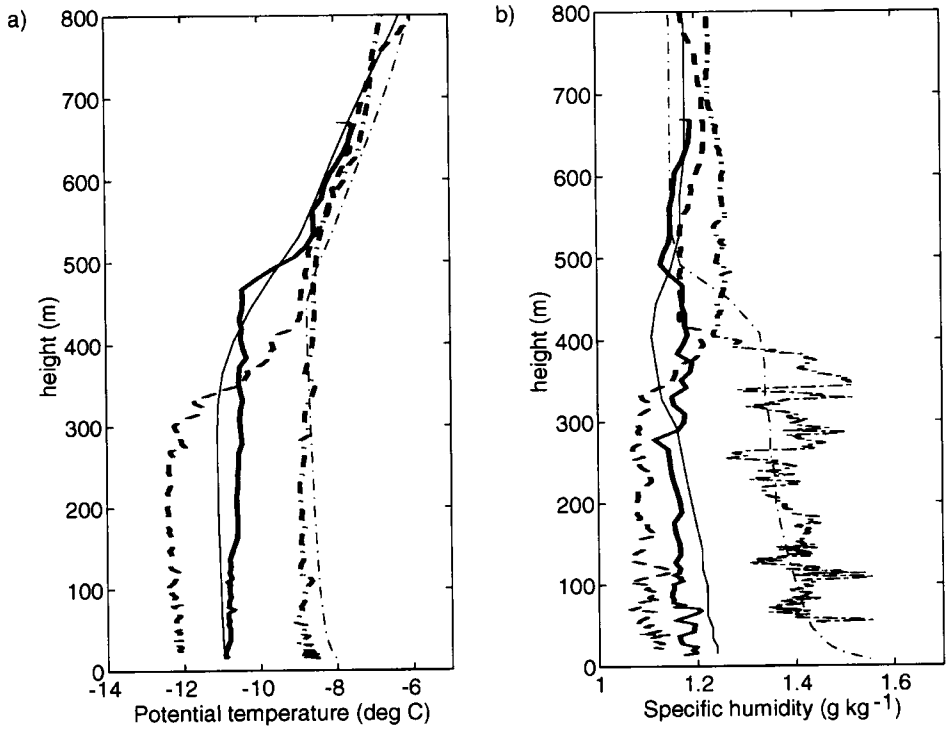

Figure 8. Observed (thick lines) and modelled (thin lines) vertical profiles of (a) air potential temperature, and (b) specific humidity at P1 (dashed line, observed profile used as the model inflow boundary condition), P4 (solid lines), and P7 (dot-dashed lines) during the off-ice flow on 5 March, 1998. See Figure 1 for the locations of P1, P4, and P7.

The observed and modelled vertical profiles of the air temperature and specific humidity are shown in Figure 8. We see that, in the lowest 300 m, the air-mass is already heated by about 1.5 °C over the fractured ice cover and the forest between P1 and P4, and this heating is rather well reproduced by the model. The inversion base at the height of 480 m at P4 is, however, not as sharp in the model results as in the observations. Still more warming, about 3 °C, takes place from P4 to P7, and this the model reproduces well. The moisture profiles are also good, except that the air above the ABL is somewhat too dry at P5.

The observed and modelled vertical fluxes at different levels at stacks I, II, and III are presented in Figure 9. The observed profiles of H and E have the shapes typical of unstable boundary layers, with maximum positive values at the surface and small values at the top of the boundary layer. In accordance with the different $(T - T_{sfc})$ values over ice and water, both the H and E fluxes are only around 20 W m^{-2} over the ice, but as large as 130 W m^{-2} and 100 W m^{-2}, respectively, over the open water at stack III. There, the sensible heat flux converges strongly between the surface and the cloud base, while the latent heat flux is almost constant through

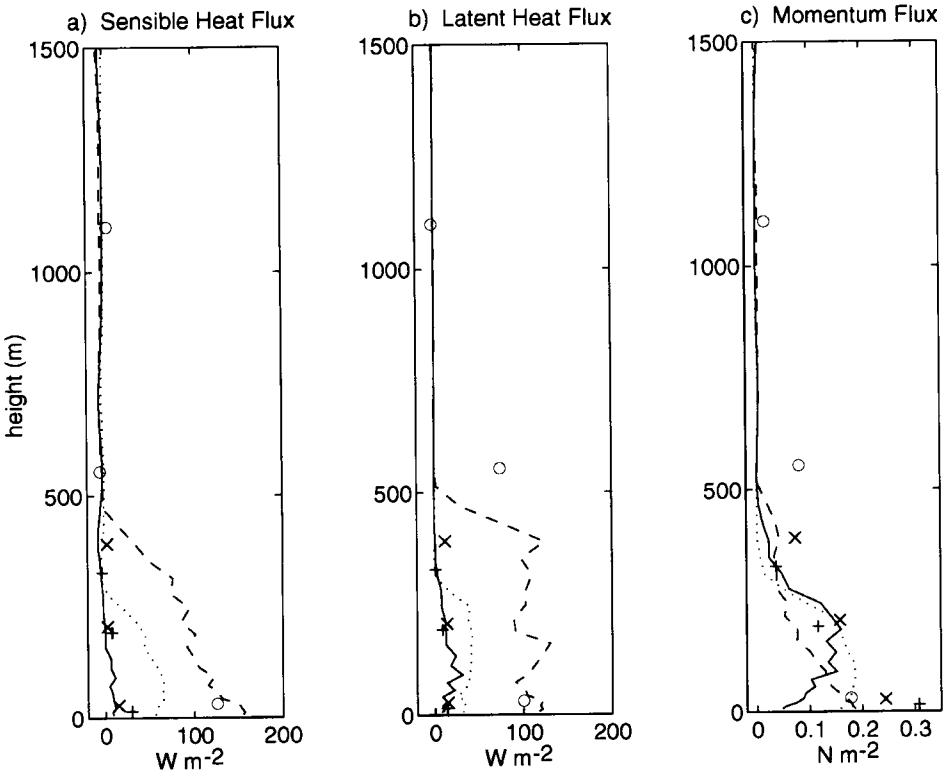

Figure 9. Observed (stack I: plus; II: cross; III: circle) and modelled (stack I: dotted lines; II: solid lines; III: dashed lines) vertical profiles of (a) sensible heat flux, (b) latent heat flux, and (c) momentum flux during the off-ice flow on 5 March, 1998.

most of the ABL and drops to zero at its top. The momentum flux is, of course, largest at the surface and decreases to zero towards the ABL top. The modelled sensible and latent heat flux profiles are reasonable at stacks II and III, but at stack I the model produces fluxes in the lowest 300 m that are too large. This is partly because the wind speed profile at the inflow boundary evolves during the 12-h simulation, and partly because the observed T and m profiles (used as fixed inflow boundary conditions) would not produce exactly the observed flux profiles, even if the wind speed profile was identical to the observations. The momentum flux profile shows unrealistic behaviour in the lowest 200 m at stack II. This is related to a flow disturbance caused by the step change in surface roughness (from the 0.8 m of the forest to the 10^{-4} m of the sea ice) one grid point upwind of stack II. At stack III, and already 16 km downwind of stack II (not shown), the profiles are reasonable, with the momentum flux increasing towards the surface. This model run, the results of which are shown in Figures 8 and 9, is referred to in the following as the reference run.

6.2. SENSITIVITY TESTS

The basically good results of the reference run were not achieved at the first modelling attempt. On the contrary, it appeared that it was important for three topics to be taken into account to reach realistic results. These were (1) recognition of the effect of the forest on the surface energy balance in the archipelago, (2) parameterization of the heat and moisture fluxes from the subgrid-scale leads within the sea ice, and (3) recognition of the presence of ice crystals in the parameterization of the air saturation humidity. To demonstrate the importance of these effects, we present four sensitivity runs: (1) Without forest but with a snow cover on the archipelago (z_0 = 0.01 m), (2) with a compact ice cover without any leads, (3) with the air saturation humidity calculated with respect to water only, and (4) neglecting all three effects: with neither forest nor leads, and the saturation calculated with respect to water only. In other respects the sensitivity runs were similar to the reference run. The principal results of the sensitivity runs are shown in Figure 10.

In run 4, the heating and growth of the boundary layer are seriously underestimated at both P4 and P7. There is very little difference between the modelled profiles at P1 and P4 (Figure 10a). Between P4 and P7 some heating takes place due to the open sea. Run 1 without forest is fine with respect to the ABL temperatures, but the ABL height is underestimated in P4: From 350 m upwards the temperature profile is close to that at P1 (Figure 10b). In run 2 without leads, the most evident results are the reduced heating and lack of ABL growth between P4 and P7 (Figure 10c). The lowest 300 m at P4 are heated less than half as much as observed. Heating from the open water upwind of P7 originates from a fetch of 15 km, which seems to be too short to cause ABL growth. In the reference run, the surface heat flux and countergradient transport through the mixed layer over the fractured ice (50 km with a 30% open water fraction) and open water cause much more boundary-layer growth between P4 and P7. The boundary-layer evolution between P1 and P4 seems to be due to the combined effect of the forest and the leads. Compared to this effect, the air-ice exchange was of smaller importance in this case.

In run 3, where the saturation was calculated with respect to water only, the air humidity was too high in the lowest 360 m at P4 (Figure 10d). In the lower levels, too high a humidity remains in the air, because the saturation humidities are higher when condensation to ice crystals is neglected. It is interesting that in run 3 the air temperature profiles (not shown) were practically as good as in the reference run: the condensation onto ice crystals does not seem to affect the ABL temperatures much in this situation, where condensation to liquid cloud droplets occurs in any case, and the radiation budget is dominated by the presence of the cloud layer.

Comparing the vertical profiles of the turbulent fluxes with the lack of leads, the sensible and latent heat fluxes were too large near the surface at P7 (the air was cold when reaching the ice edge). In sensitivity run 4, both the evaporation and boundary-layer growth were reduced and the latent heat flux already fell to zero at a height of 350 m.

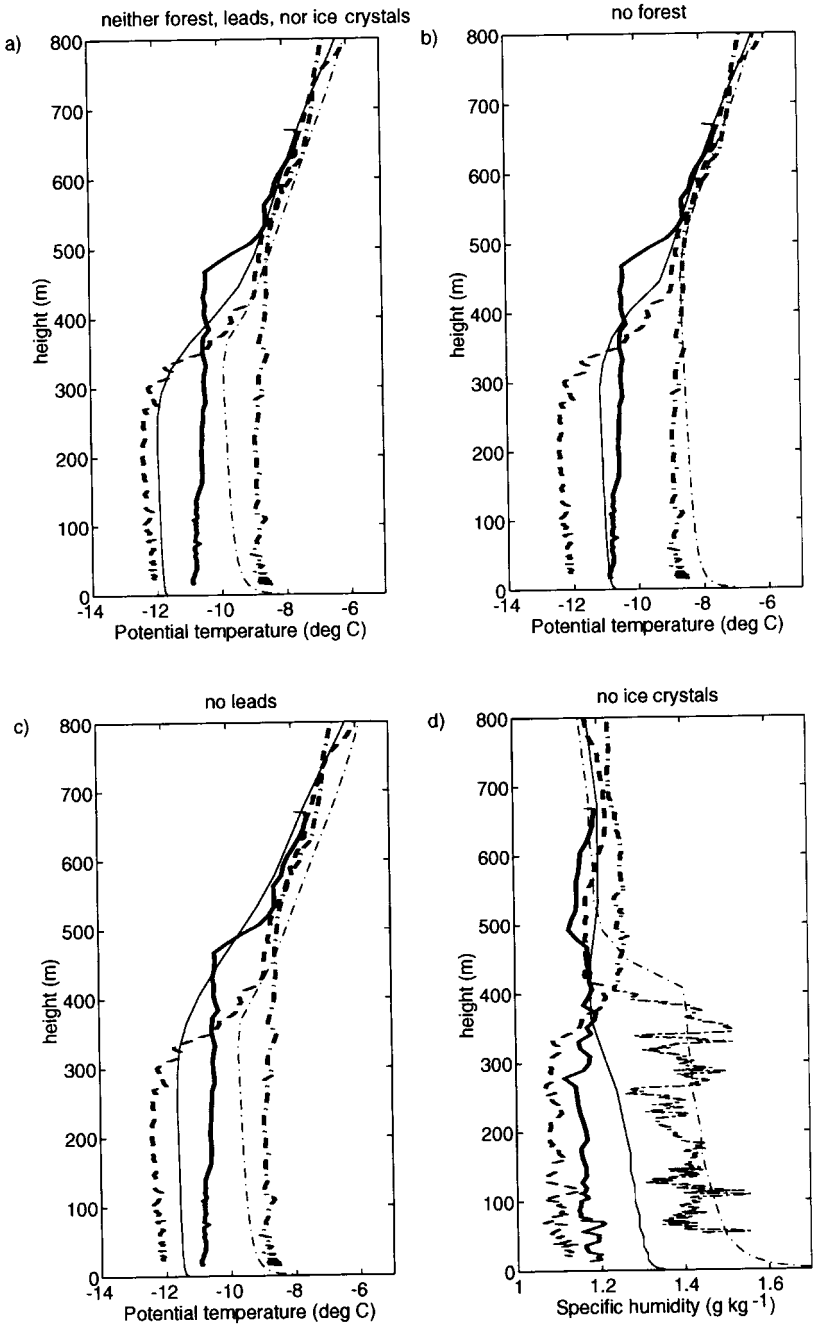

Figure 10. Observed (thick lines) and modelled (thin lines) vertical profiles of air potential temperature in (a) sensitivity run 4, (b) run 1, and (c) run 2, and (d) specific humidity in run 3, at P1 (dashed line; observed profile used as the model inflow boundary condition), P4 (solid lines), and P7 (dot-dashed lines) during the off-ice flow on 5 March, 1998.

6.3. HEAT AND MOISTURE BUDGET

We estimate the heat and moisture budget in the lowest 300 m, between stacks I and II and between stacks II and III, on the basis of the observations and model results. Assuming a well-mixed ABL, no radiative cooling, no water phase changes, and cross-flow homogeneity ($\partial/\partial y = 0$), we can simplify the budget equations as follows:

$$\frac{\partial \theta}{\partial t} = -u\frac{\partial \theta}{\partial x} - w\frac{\partial \theta}{\partial z} - \frac{1}{\rho_p}\frac{\partial H}{\partial z}, \tag{1}$$

$$\frac{\partial m}{\partial t} = -u\frac{\partial m}{\partial x} - w\frac{\partial m}{\partial z} - \frac{1}{\rho L}\frac{\partial E}{\partial z}, \tag{2}$$

where θ is the potential temperature of the air and L is the latent heat of condensation. Our estimates for each term in the budget are listed in Table I. We first look at the observed budgets. The vertical advection term is assumed to vanish, since both θ and m are well-mixed in the lowest 300 m, and their vertical gradients accordingly approximately vanish. Both over ice (stacks I–II) and water (stacks II–III) horizontal advection causes a cooling and drying of the air, whereas the turbulent fluxes cause a warming and moistening of the air in the lowest 300 m. Generally, the horizontal advection term dominates and determines the sign of the local time derivative. The magnitudes of the horizontal advection and the turbulent flux divergence are about twice as large over the open water compared with those over the ice, except for the latent heat flux divergence. The calculated budgets can be compared with the rawinsonde sounding profiles over the R/V Aranda ice station (Figure 1) at stack II at 0830 and 1130 UTC. In the soundings, the temperature in the lowest 300 m decreased by 0.3 K in 3 h, yielding $\partial\theta/\partial t = -0.1$ K h^{-1}, and the mixing ratio decreased by 0.02 g kg^{-1} in 3 h, yielding $\partial m/\partial t = -0.007$ g kg^{-1} h^{-1}.

The main difference between the modelled budgets and those based on the Falcon observations is that in the model the time derivatives vanish, as the model was run into a steady state. Thus, the horizontal advection of cold air is balanced by the vertical heat flux convergence, and the advection of dry air is balanced by the vertical moisture flux convergence, with minor contributions from the vertical advection terms. The modelled $\partial\theta/\partial t$ and $\partial m/\partial t$ are very close to those based on the rawinsonde soundings. All three methods give a practically stationary moisture budget between stacks I and II, between stacks II and III, we did not model the temporal evolution of the off-ice flow. The differences between the observed and modelled budgets may also have arisen from the assumptions made in deriving (1) and (2). For a more detailed analysis of the budget terms during an air-mass modification, see Lenschow (1973).

TABLE I

Estimate of heat and moisture budgets in the lowest 300 m between stacks I–II and II–III.

	Stacks I–II		Stacks II–III	
	Observed	Modelled	Observed	Modelled
$-u\ \partial\theta/\partial x$ (K h^{-1})	−0.69	−0.34	−1.29	−0.95
$-w\ \partial\theta/\partial z$ (K h^{-1})	0	0.03	0	−0.01
$-(1/\rho c_p)\ \partial H/\partial z$ (K h^{-1})	0.23	0.31	0.64	0.96
$\partial\theta/\partial t$ (K h^{-1})	−0.46	0.0	−0.65	0.0
$-u\ \partial m/\partial x$ (g kg^{-1} h^{-1})	−0.054	−0.050	−0.11	−0.069
$-w\ \partial m/\partial z$ (g kg^{-1} h^{-1})	0	0.002	0	−0.009
$-(1/\rho L)\ \partial E/\partial z$ (g kg^{-1} h^{-1})	0.055	0.048	0.055	0.078
$\partial m/\partial t$ (g kg^{-1} h^{-1})	0	0.0	−0.055	0.0

7. Discussion

We have presented two cases of air flow over the ice-edge zone: On-ice and off-ice flow. They represent the two opposite situations occurring in wintertime over the ice edge zone in the Baltic Sea. The stable boundary layer during the on-ice flow exhibited little thermal modification but interesting wind features, due to the frictional decoupling with the surface. During the off-ice flow, the coupling between the surface and the air was strong, and hence the boundary layer became strongly unstable over the open water and the thermal modification was large. Common to both cases was, however, the importance of the vicinity of the land surface on the ABL.

During on-ice flows in general, the ABL over the upwind open sea is typically close to thermal equilibrium with the surface. After crossing the ice edge, the warm air mass provides heat to the snow surface, and the snow temperature increases. This process had apparently already taken place before the Falcon observations on 27 February, 1998, as southerly winds had prevailed for two days before the flight mission. The air-surface temperature difference and the turbulent exchange were therefore small over the ice. Hence, in contrast to the case of 5 March, the results of this case were not sensitive to the parameterization of the subgrid-scale heat and moisture fluxes. If the ice surface is colder, a larger downward heat flux and stronger air-mass modification may, however, take place during on-ice flows (Andreas et al., 1984).

The wind field showed a low-level jet (LLJ) that was most pronounced over the ice. Similar wind conditions are often observed in stable boundary layers (e.g., Brümmer at al., 1994), and they can lead to wind shears causing inflection point instability (Brümmer and Latif, 1985). In the model, the overall shape of the wind profile well above the SBL was related to baroclinicity, but the LLJ at the height

of 250 m was associated with inertial oscillations. The mechanism is a spatial analogy to the classical nocturnal jet development in time, and is in agreement with the observations of Högström and Smedman (1984) and Smedman et al. (1993) over the open Baltic Sea in spring and summer. Although an LLJ associated with inertial oscillations is a well-known feature in stable boundary layers, relatively few studies have so far documented it over sea ice. Andreas et al. (2000) do so, but in their case over the Weddell Sea it was the onset of stable stratification, not spatial differences, that triggered the jets. A few studies have shown other mechanisms for the generation of LLJs over the sea ice or its edge zone: the ice breeze (Langland et al., 1989), baroclinicity as the main mechanism (Vihma et al., 1998), and katabatic or barrier winds (King and Turner, 1997).

Although the observed LLJ was most pronounced over the ice, the modelling suggests that the jet was not generated by the ice edge but by the coastline, where a much more drastic change in the thermal stratification and surface roughness took place. The observed and modelled location of the maximum jet approximately 500 km from the coast followed the theory of Thorpe and Guymer (1977). Further, in the modelling study without the land surface, the LLJ was not a stationary feature: it was only maintained for as long a time as the advection of the inflow air mass through the model domain lasted. The generation, maintenance, and strength of the LLJ was very sensitive to the parameterization of turbulent mixing in the model. In particular, the value for ϵ in the equation for the mixing length, and the stability dependence of the transfer coefficients in the interior of the ABL (not at the surface), were important.

In the case of the off-ice flow on 5 March, 1998, the modification of the airmass and the development of a convective boundary layer over the open sea were reasonably well simulated by the two-dimensional mesoscale model. The sensitivity runs suggested that in this case it was essential to take into account the effects on the ABL of the subgrid-scale leads and the archipelago forest. The local surface sensible heat flux over leads was up to 120 W m^{-2}, yielding grid-averaged sensible heat fluxes of about 40 W m^{-2}. These fluxes were particularly important for the heating of the ABL. Without the forest these large fluxes were not, however, effective enough to reproduce the observed growth of the ABL at P4. In the presence of the forest in the archipelago, the boundary-layer growth was better simulated, and, even without the leads, the forest, together with the small upward heat flux from the ice, provided half of the heating observed at P4. The treatment of the forest still requires, however, further studies: this can be seen from the disturbed momentum flux profiles at the downwind edge of the forest. Results comparable to ours were recently obtained from the southern Baltic Sea, where Gryning and Batcharova (2002) observed that the island of Bornholm caused an increase in the boundary-layer height downwind of it.

The aircraft observations indicated that ice crystals were present over almost the entire experimental area on 5 March. Taking them into account in a very simple manner, by calculating the saturation humidity as the average of saturation

with respect to water and ice, clearly improved the modelled humidity profile at P4. In addition to the sensitivity tests described in detail, we may note that the countergradient transport was important for the heating and growth of the ABL at P7, where the convection was strongest. This effect has been well documented in several studies (Chrobok et al., 1992; Lüpkes and Schlünzen, 1996).

Acknowledgements

We are grateful to colleagues participating in the Baltic Air-Sea-Ice Study co-ordinated by Jouko Launiainen. The discussions with Mikael Magnusson and the assistance by David Schröder, Stefan Thiemann, Bin Cheng, and Roberta Pirazzini are acknowledged. Maria Lundin provided us with the MESAN fields and sea ice concentrations from the SMHI. TV is grateful to Hannu Savijärvi for his advice in mesoscale modelling. The study was supported by the European Commission under the contract MAST3-CT97-0117 (BALTEX-BASIS).

References

Alestalo, M. and Savijärvi, H.: 1985, 'Mesoscale Circulations in a Hydrostatic Model: Coastal Convergence and Orographic Lifting', *Tellus* **37A**, 156–162.

Andersson, T. and Gustafsson, N.: 1994, 'Coast of Departure and Coast of Arrival: Two Important Concepts for the Formation and Structure of Convective Snowbands over Seas and Lakes', *Mon. Wea. Rev.* **122**, 1036–1049.

Andersson, T. and Michelson, D. B.: 1999, 'The December 1998 Snowfall over Sweden as Seen by Weather Radars', *Polarfront*, Swedish Meteorological Society, Norrköping, No. 100–101, pp. 26–33.

Andreas, E. L., Claffey, K. J., and Makshtas, A. P.: 2000, 'Low-Level Atmospheric Jets and Inversions over the Weddell Sea', *Boundary-Layer Meteorol.* **97**, 459–486.

Andreas, E. L., Tucker III, W. B., and Ackley, S. F.: 1984, 'Atmospheric Boundary-Layer Modification, Drag Coefficient, and Surface Heat Flux in the Antarctic Marginal Ice Zone', *J. Geophys. Res.* **89**, 649-661.

Bennett, Jr., T. J. and Hunkins, K.: 1986, 'Atmospheric Boundary Layer Modification in the Marginal Ice Zone', *J. Geophys. Res.* **91**, 13033–13044.

Buck, A. L.: 1981, 'New Equations for Computing Vapour Pressure and Enhancement Factor', *J. Appl. Meteorol.* **20**, 1527–1532.

Brümmer, B.: 1997, 'Boundary Layer Mass, Water, and Heat Budgets in Wintertime Cold-Air Outbreaks from the Arctic Sea Ice', *Mon. Wea. Rev.* **125**, 1824–1837.

Brümmer, B. and Latif M.: 1985, 'Some Studies on Inflection Point Instability', *Contr. Atmos. Phys.* **58**, 117–126.

Brümmer, B. and Müller, G.: 1999, 'Boundary Layer Measurements with Research Aircraft Falcon', in J. Launiainen (ed.), *BALTEX-BASIS Data Report 1998, Int. BALTEX Secretariat Publ.*, Vol. 1, Geesthacht, Germany, pp. 26–38.

Brümmer, B., Busack, B., Hoeber, H., and Kruspe, G.: 1994, 'Boundary-Layer Observations over Water and Arctic Sea Ice During On-Ice Air Flow', *Boundary-Layer Meteorol.* **68**, 75–108.

Cheng, B., Launiainen, J., Vihma, T., and Uotila, J.: 2001, 'Modelling Sea Ice Thermodynamics in BALTEX-BASIS', *Ann. Glaciol.*, in press.

Chrobok, G., Raasch, S., and Etling, D.: 1992, 'A Comparison of Local and Non-Local Turbulence Closure Methods for the Case of a Cold Air Outbreak', *Boundary-Layer Meteorol.* **58**, 69–90.

Gustafsson, N., Nyberg, L., and Omstedt, A.: 1998, 'Coupling of a High-Resolution Atmospheric Model and an Ocean Model for the Baltic Sea', *Mon. Wea. Rev.* **126**, 2822–2846.

Gryning, S.-E. and Batchvarova, E.: 2002, 'Marine Boundary Layer and Turbulent Fluxes over the Baltic Sea: Measurements and Modelling', *Boundary-Layer Meteorol.* **103**, 29–47.

Gryning, S.-E., Batchvarova, E., and De Bruin, H. A. R.: 2001, 'Energy Balance of a Sparse Coniferous High-Latitude Forest under Winter Conditions', *Boundary-Layer Meteorol.* **99**, 465–488.

Häggmark, L., Ivarsson, K. I., Gollvik, S., and Olofsson, P. O.: 2000, 'Mesan, an Operational Mesoscale Analysis System', *Tellus* **52A**, 2–20.

Hartmann, J., Kottmeier, C., and Raasch, S.: 1997, 'Roll Vortices and Boundary-Layer Development During a Cold Air Outbreak', *Boundary-Layer Meteorol.* **84**, 45–65.

Högström, U.: 1988, 'Non-Dimensional Wind and Temperature Profiles in the Atmospheric Surface Layer: A Re-Evaluation', *Boundary-Layer Meteorol.* **42**, 55–78.

Högström, U. and Smedman, A.-S.: 1984, 'The Wind Regime in Coastal Areas with Special Reference to Results Obtained from Swedish Wind Energy Program', *Boundary Layer Meteorol.* **30**, 351–373.

Holtslag, A. A. M. and de Bruin, H. A. R.: 1988, 'Applied Modeling of the Nighttime Surface Energy Balance over Land', *J. Appl. Meteorol.* **37**, 689–704.

Holtslag, A. A. M. and Moeng, C.-H.: 1991, 'Eddy Diffusivity and Countergradient Transport in the Convective Atmospheric Boundary Layer', *J. Atmos. Sci.* **48**, 1690–1698.

Joffre, S. M.: 1982, 'Momentum and Heat Transfers in the Surface Layer over a Frozen Sea', *Boundary-Layer Meteorol.* **24**, 211–229.

Joffre, S. M.: 1983, 'Determining the Form Drag Contribution to the Total Stress of the Atmospheric Flow over Ridged Sea Ice', *J. Geophys. Res.* **88**, 4524–4530.

Källstrand, B.: 1998, 'Low Level Jets in a Marine Boundary Layer during Spring', *Contr. Atmos. Phys.* **71**, 359–373.

King, J. C. and Turner, J.: 1997, *Antarctic Meteorology and Climatology*, Cambridge University Press, Cambridge, U.K., 409 pp.

Langland, R. H., Tag, P. M., and Fett, R. W.: 1989, 'An Ice Breeze Mechanism for Boundary-Layer Jets', *Boundary-Layer Meteorol.* **48**, 177–195.

Launiainen, J. (ed.): 1999, *BALTEX-BASIS Data Report 1998, Int. BALTEX Secretariat Publ.*, Vol. 14, Geesthacht, Germany, 94 pp.

Launiainen, J. and Cheng, B.: 1998, 'Modelling of Ice Thermodynamics in Natural Water Bodies', *Cold Reg. Sci. Tech.* **27**, 153–178.

Launiainen, J. and Laurila, T.: 1984, 'Marine Wind Characteristics in the Northern Baltic Sea', *Finnish Marine Res.* **250**, 52–86.

Launiainen, J., Cheng, B., Uotila, J., and Vihma, T.: 2001, 'Turbulent Surface Fluxes and Air-Ice Coupling in BASIS', *Ann. Glaciol.* in press.

Lenschow, D. H.: 1973, 'Two Examples of Planetary Boundary Layer Modification over the Great Lakes', *J. Atmos. Sci.* **30**, 568–581.

Lüpkes, C. and Schlünzen, K. H.: 1996, 'Modelling the Arctic Convective Boundary-Layer with Different Turbulence Parameterizations', *Boundary-Layer Meteorol.* **79**, 107–130.

Mahrt, L.: 1981, 'Modelling the Depth of the Stable Boundary Layer', *Boundary-Layer Meteorol.* **21**, 3–19.

Mai, S., Wamser, C., and Kottmeier, C.: 1996, 'Geometric and Aerodynamic Roughness of Sea Ice', *Boundary-Layer Meteorol.* **77**, 233–248.

Ni, W. and Woodcock, C. E.: 2000, 'Effect of Canopy Structure and the Presence of Snow on the Albedo of Boreal Conifer Forests', *J. Geophys. Res.* **105**, 11879–11888.

Olsson, P. Q. and Harrington, J. Y.: 2000, 'Dynamics and Energetics of the Cloudy Boundary Layer in Simulations of Off-Ice Flow in the Marginal Ice Zone', *J. Geophys. Res.* **105**, 11889–11899.

Raasch, S.: 1990, 'Numerical Simulation of the Development of the Convective Boundary Layer during a Cold Air Outbreak', *Boundary-Layer Meteorol.* **52**, 349–375.

Renfrew, I. A. and Moore, G. W. K.: 1999, 'An Extreme Cold Air Outbreak over the Labrador Sea: Roll Vortices and Air-Sea Interaction', *Mon. Wea. Rev.* **127**, 2379–2394.

Savijärvi, H.: 1991, 'The United States Great Plains Diurnal ABL Variation and the Nocturnal Low-level Jet', *Mon. Wea. Rev.* **119**, 833–840.

Savijärvi, H.: 1997, 'Diurnal Winds around Lake Tanganyika', *Quart. J. Roy. Meteorol. Soc.* **123**, 901–918.

Savijärvi, H. and Alestalo, M.: 1988, 'Sea Breeze over a Lake or Gulf as the Function of the Prevailing Flow', *Contr. Atmos. Phys.* **61**, 98–104.

Smedman, A.-S., Tjernström, M., and Högström, U.: 1993, 'Analysis of the Turbulence Structure of a Marine Low-Level Jet', *Boundary-Layer Meteorol.* **66**, 105–126.

Smith, S. D.: 1988, 'Coefficients for Sea Surface Wind Stress, Heat Flux, and Wind Profiles as a Function of Wind Speed and Temperature', *J. Geophys. Res.* **93**, 15,467–15,472.

Thorpe, A. J. and Guymer, T. H.: 1977, 'The Nocturnal Jet', *Quart. J. Roy. Meteorol. Soc.* **103**, 633–653.

Uotila, J., Vihma, T., and Launiainen, J.: 1997, *Marine Meteorological Radiosoundings in the Northern Baltic Sea from R/V Aranda in 1994-95, Meri, Report Series of The Finnish Institute of Marine Research*, Vol. 30, 57 pp.

Vihma, T.: 1995, 'Subgrid Parameterization of Surface Heat and Momentum Fluxes over Polar Oceans', *J. Geophys. Res.* **100**, 22,625–22,646.

Vihma, T. and Kottmeier, C.: 2000, 'A Modelling Approach for Optimizing Flight Patterns in Airborne Meteorological Measurements', *Boundary-Layer Meteorol.* **95**, 211–230.

Vihma, T. and Savijärvi, H.: 1991, 'On the Effective Roughness Length for Heterogeneous Terrain', *Quart. J. Roy. Meteorol. Soc.* **117**, 399–407.

Vihma, T., Uotila, J., Cheng, B., Purokoski, T., Kosloff, P., Launiainen, J., and Schrum, C.: 1999, 'Marine Meteorological, Sea Ice and Oceanographic Observations by the Finnish Institute of Marine Research', in J. Launiainen (ed.), *BALTEX-BASIS Data Report 1998, Int. BALTEX Secretariat Publ.*, Vol. 14, Geesthacht, Germany, pp. 14–25.

Vihma, T., Uotila, J., and Launiainen, J.: 1998, 'Air-sea Interaction over a Thermal Marine front in the Denmark Strait', *J. Geophys. Res.* **103**, 27,665–27,678.

Wu, J.: 1980, 'Wind Stress Coefficients over Sea Surface, a Revisit', *J. Phys. Oceanog.* **10**, 727–740.